Influence of on-board produced hydrogen and three way catalyst on soot nanostructure in Gasoline Direct Injection engines

Bogarra Macias, Maria; Herreros, Jose; Tsolakis, Athanasios; York, Andrew; Millington, Paul; Francisco, Martos

DOI:
10.1016/j.carbon.2017.05.049

Document Version
Peer reviewed version

Citation for published version (Harvard):
Bogarra Macias, M, Herreros, J, Tsolakis, A, York, A, Millington, P & Francisco, M 2017, 'Influence of on-board produced hydrogen and three way catalyst on soot nanostructure in Gasoline Direct Injection engines', *Carbon*, vol. 120, pp. 326-336. https://doi.org/10.1016/j.carbon.2017.05.049

Influence of On-Board Produced Hydrogen and Three Way Catalyst on Soot Nanostructure in Gasoline Direct Injection Engines

M. Bogarra[a], J.M. Herreros[a], A. Tsolakis[a*], A.P.E. York[b], P.J. Millington[b], and F.J. Martos[c]

[a]*School of Mechanical Engineering, University of Birmingham, Edgbaston, B15 2TT, UK*

[b]*Johnson Matthey Technology Centre, Blount's Court, Sonning Common, Reading, RG4 9NH, UK*

[c]*Escuela Técnica Superior de Ingeniería Industrial, University of Málaga, 29071, Málaga, Spain*

Abstract

Effectively controlling carbon soot emission from Gasoline Direct Injection (GDI) engines to achieve legislative emission limits is a challenge for both the vehicle manufacturers and researchers. Transmission electron microscopy is a powerful tool for obtaining morphological and nanostructural parameters of carbon soot in Particulate Matter (PM) emissions. These parameters play a significant role in PM emissions control as are affecting filtration efficiency and soot oxidation characteristics.

In this paper, a comprehensive analysis of the interlayer spacing, fringe length and fringe tortuosity (curvature) of primary soot particles from GDI engine has been performed. GDI primary particles showed a core-shell structure, similar to diesel soot, with an inner core diameter between 6 and 16 nm and the outer graphene layer between 6 and 13 nm. The soot nanostructure is not significantly modified by changing the fuel injection timing or by introducing EGR and hydrogen in the combustion process. These results are opposed to those obtained from soot emitted in diesel engines where soot nanostructure is affected with changes in engine operating conditions. Furthermore, the three way catalytic converter does not influence soot nanostructure or the soot oxidation characteristics.

Keywords: GDI, PM, TEM, EGR, REGR, TWC, nanostructure, fringe length, tortuosity, interlayer spacing.

*Corresponding author. Tel.: +44 (0) 121 414 4170. E-mail address: a.tsolakis@bham.ac.uk (A. Tsolakis).

1. INTRODUCTION

By 2020, the European Union has imposed a CO_2 target of 95 g/km for passenger cars [1]. Gasoline Direct Injection (GDI) engines technology has the potential of substantially improving overall vehicle fuel economy and thus, reducing CO_2 [2]. However, GDI engines increase the level of particulate matter (PM) emissions in both mass and number compared to previous gasoline technologies. PM in diesel engines is considered carcinogenic to humans [3] and it is linked with cardiopulmonary inflammation [4] and respiratory problems [5]. Legislations, such as the Euro 6c (September 2017), limits the number of particles per kilometre, therefore, the use of Gasoline Particulate Filters (GPFs) may be required [6]. In order to avoid an increase of fuel consumption due to the increased backpressure of loaded GPFs, the regeneration events must be accurately controlled [7]. Therefore, the understanding of soot structure, morphology and oxidation characteristics is important in developing control strategies. As diesel engines have been the main source of PM, strong efforts have been made to characterise PM properties using transmission electron microscopy (TEM) [8-13].

Soot nanostructure is related to particle formation history in the combustion chamber [14] and its dependent of the initial fuel [15]. Also, soot surface chemistry, which it is linked to soot's environmental and health impact, is dependent on its nanostructure [16, 17]. Furthermore, soot reactivity, defined as the ease to oxidise mature soot [9], depends on its physicochemical properties. The morphology, nanostructure, chemical functional groups and ash content has been reported to impact the soot oxidation characteristics [8, 9, 15, 16, 18, 19], although there is no clear agreement about the contribution of each property [18]. In diesel engines, it is thought that soot properties can be altered, in order to produce a more reactive soot resulting in less demanding regeneration events in diesel particulate filters [8, 9]. The same idea should apply to GPFs. However, for GDI engines, soot nanostructure knowledge is still scarce.

Most of the literature describes qualitatively the nanostructural properties of PM emitted by GDI engines, but, not many studies report findings on parameters such as interlayer spacing, crystallite length or curvature (tortuosity) of primary carbon particles. For instance, Uy et al. [20] studied the nanostructure of soot-in-oil and soot scrapped from the exhaust pipe under different driving conditions, It was reported that the thickness of the shell structure lay from 5 to 8 nm. Plane defects were found in the particles (not smooth edges). Sludge-like particles were observed, the amorphous appearance of those particles is attributed to decomposition under the TEM beam [20]. Comparing diesel and GDI soot, three main differences were found: i) GDI soot is composed by higher quantities

of Ca and Zn (from oil additive and wear) than in diesel samples, ii) GDI soot-in-oil is less structured and more “sludge-like” in appearance, and iii) polyaromatic hydrocarbons (PAHs) adsorbed in GDI soot differ in quantity and structure compared to diesel. Wang-Hansen et al. [21] concluded that the nanostructure of soot was similar to diesel, with an inner part showing concentric layers and turbostratic structure. Although the dissimilar oxidative behaviour of gasoline soot is attributed to the variations in crystallite layer plane dimensions, no nanostructural parameters were quantified. Seong et al. [22] analysed soot nanostructure from a GDI engine operating at range of loads and fuel injection timings at stoichiometric air to fuel ratio. It was reported that the soot nanostructure was less-ordered than diesel soot or carbon black, although at high loads GDI soot had a graphitic structure. The authors argued that the quantity of hydrocarbons (HCs) during PM formation was limited and therefore, the graphitisation process was reduced. In follow-up research work from the same authors [23], the GDI PM nanostructure was analysed using high resolution TEM (HRTEM) and Raman at three engine conditions including cold start. A similar concentric pattern and carbon nanostructure was reported for all the conditions analysed, thus no significant differences were found between HRTEM and Raman analysis. GDI soot presented well-defined concentric fringes even at engine cold start. The Raman spectra was similar for all the engine conditions studied, showing that GDI soot nanostructure is less dependent on the engine condition than diesel soot due to the more homogeneous conditions characteristic of the gasoline combustion. La Rocca et al. [24] collected samples after 30 hours running at different engine conditions. Three different layers in the nanostructure were distinguished: (i) an inner core (25nm thick), (ii) a middle onion-like structure (8-12nm thick) and (iii) an outer more amorphous layer (5nm thick). The presence of this external amorphous layer was thought to increase the edge sites and therefore, the GDI soot reactivity. Gaddam et al. [19] carried out an in-depth physical and chemical analysis of gasoline PM using TEM, X-ray photoelectron spectroscopy, and Fourier Transform Infrared – Attenuated Total reflectance in a single cylinder GDI engine. Longer fringe lengths and reduced tortuosity in the soot nanostructure were reported under lean in fuel conditions. . The authors state that in the areas of the combustion chamber where the equivalence ratio was lower from the critical for soot formation, soot growth and C5 species addition was avoided, leading to reduced tortuosity. Miyashita et al. [25] observed that the interlayer spacing was increased with fuel availability during the formation process. The authors concluded that these values are characteristic of upstream in-flame diesel soot formed at relatively low temperatures (~1600K). Liati et al. [26] analysed the nanostructure of GDI soot produced during the New European Driving Cycle and World harmonised Light vehicles Test Cycle at normal and low temperatures. For all the driving cycles analysed, the primary particle nanostructure showed an outer rig formed by graphene lamellae and the presence of amorphous

material. Similarly to previous references, the inner part of the particle is amorphous. In general, it has been reported in the literature that GDI soot presents less ordered structure than diesel [20, 22, 23] and therefore is more reactive [26]. Irregular patterns [22], inter connected fringes [23] and turbostatic structure, similar to diesel soot [20, 21, 24], are characteristics of GDI soot.

The effect of exhaust gas recirculation (EGR) has been widely analysed for diesel engines, although discrepancies can be found in the literature regarding its effect on PM nanostructure [8, 27]. However, for GDI engine, the influence of EGR on nanostructure has not been documented yet. In this research, GDI soot nanostructure parameters (interlayer spacing, fringe length and fringe tortuosity) have been obtained following the methods used in the diesel literature [10-12, 16]. For first time, the effect of high EGR percentages on GDI soot nanostructure has been assessed and compared to reformate gas exhaust recirculation (REGR) conditions. REGR is a technique that utilises the heat from the exhaust, water and carbon dioxide to produce a rich-in-hydrogen gas on board, which can then be recirculated back to the engine for combustion. It is expected that the high temperatures (600-700°C) seen in the fuel reforming reactor and the catalyst presence could modify the soot nanostructure or even eliminate soot fed back to the engine. Furthermore, the TWC influence on nanostructure has also been studied here for baseline conditions (noEGR).

2. EXPERIMENTAL SETUP AND METHODOLOGY

2.1.Experimental setup

The engine used for this study is a 2L, 4-cylinder, air-guided GDI. A steady-state condition corresponding to a medium-load point of the NEDC was selected: 2100 rpm engine speed and 4.7 bar indicated mean effective pressure (IMEP). The details of the engine specification can be found in Table 1. Standard EN228 gasoline with 5% (v/v) ethanol content provided by Shell was used for this research (Table 2).

Table 1. Engine specifications.

Compression Ratio	10:1
Bore x Stroke	87.5 x 83.1 mm
Turbocharger	Borg Warner K03
Rated Power	149 kW At 6000 rpm
Rated Torque	300 Nm At 1750-4500 rpm
Engine Management	Bosch Me17

Table 2. Gasoline properties.

Analysis (Test method)		Unit	Result
Density at 15ºC (DIN EN ISO 12185)		kg/m^3	743.9
Distillation (DIN EN ISO 3405)	IBP	ºC	34.6
	20% v/v	ºC	55.8
	50% v/v	ºC	94.0
	FBP	ºC	186.3
C		m/m %	84.16
H		m/m %	13.48
O		m/m %	2.36
Paraffins		% vol	43.9
Olefins		% vol	11.7
Naphthenes		% vol	7.8
Aromatics		% vol	26.9
Oxygenates		% vol	7.7
Sulfur		ppm	6
Lower Heating Value (DIN 51603-1)		MJ/kg	42.22
MON (DIN EN ISO 5163)		85.3	85.3
RON (DIN EN ISO 5164)		96.5	96.5

For nanostructural analysis 3.05 mm, TAAB Formvar coated copper grids were loaded directly from the exhaust pipe. The sampling line was heated to avoid water/HC condensation but no dilution was used. A 200 kV FEI Talos™ F200X scanning/ transmission electron microscope (S/TEM) was used in this investigation.

2.2.Test procedure and methodology

2.2.1. Test procedure

The nature of the engine out PM was modified by using two different fuel injection timing settings i) small soot nuclei and volatile organic compounds (303 CAD bTDC, ECU settings) and ii) highly sooty particles (335 CAD bTDC, advanced injection setting). In previous work [28], it was reported that advanced fuel injection settings produced ten times higher PM concentration than normal ECU settings. The thermogravimetric analysis (TGA) showed a 98% solid soot with 2% content in volatile material under early injection timing [28].

The analysis was carried out at the maximum percentage of EGR rates, 19% and 24%, that the engine could tolerate, while maintaining the coefficient of variation (COV) below 5% for injection timings of 303 CAD bTDC and 335 CAD bTDC, respectively. In order to compare the REGR with EGR, the same dilution rates were utilised. The maximum position of the in-cylinder pressure was maintained in a ±3 CAD narrow window for all the engine conditions. These combustion settings are summarised in Table 3 where the percentage of EGR/REGR, spark timing per condition and the

maximum peak pressure position compared to the baseline are reported. 200 cycles were considered for obtaining these values. Stoichiometric lambda was maintained for all the engine conditions tested.

Table 3. Engine settings for noEGR, EGR and REGR at both injection timings: 303 and 335 CAD bTDC.

Injection timing	Dilution	Spark timing (CAD bTDC)	COV of IMEP (%)	IMEP	Position Pmax (CAD)
303 CAD bTDC	noEGR	+ 24 (ECU)	2.03	4.7	16
	EGR (19%)	+ 32.25 (+ 8.25*)	4.35	4.71	16
	REGR (19%)	+ 27.75 (+ 3.75*)	3.33	4.62	16
335 CAD bTDC	noEGR	+ 24 (ECU)	1.2	4.71	12
	EGR (24%)	+ 41.25 (+ 17.25*)	5.22	4.69	12
	REGR (24%)	+ 23.25 (- 0.75*)	2.97	4.63	12

(*) + advance, - retard, spark timing with respect to ECU settings.

The commercial TWC used in this work meets the Euro 6 legislation. The on-board reformer designed by Johnson Matthey consists of five metallic plates coated with Pt – Rh based catalyst. For the reforming process, part of the exhaust gas flow before the TWC is diverted to the catalytic input of the reformer. In this stream, gasoline is injected for the reforming reactions. The rest of the exhaust stream is treated by the TWC and then used for the second inlet of the reformer to heat up the reforming catalyst. Heat exchange, but not mass exchange, is produced in the reformer between both exhaust gas streams, increasing the temperature of the catalysed exhaust + gasoline stream and therefore, promoting endothermic reforming reactions between the gasoline and hot exhaust gas [29]. The reforming process products are mainly hydrogen and CO that were recirculated back to the engine intake. This process is known as REGR. 5% hydrogen was produced in the reforming process together with some hydrocarbon species such as methane, propane and toluene. Further information about the reforming process and species can be found in references [30, 31].

2.2.2. Particle nanostructure methodology

The nanostructural properties analysed in this work are: interlayer spacing (d_{002}), graphene lamellae width (L_a) and tortuosity (τ). These parameters have already been used in the diesel literature due to its relationship with soot oxidation behaviour [10-12, 16], although the importance of each parameter is still not well understood [32]. These are analysed under baseline conditions, EGR and REGR at 303 CAD bTDC and 335 CAD bTDC fuel injection timings. The influence of the TWC on soot nanostructure was also assessed at baseline conditions for both fuel injection timings.

The interlayer spacing is a measurement of the degree of graphitisation [33] and it has been calculated following Equation 1. For each condition, at least 40 graphene lamellae stacks (L_c) were measured in four micrographs randomly located in different grid sections [8, 34]. Only graphene lamellae in the outskirt of the particles were considered [8].

$$d_{002} = \frac{L_c}{\kappa - 1} \quad [1]$$

Where L_c is the fringe or stacking height and κ the number of layers measured.

The fringe length or crystallite basal plane diameter is a measure of the physical extent of the atomic carbon layer [11, 16]. It has been reported that smaller values of L_a are related with higher soot reactivity [11].

The tortuosity or wavy structure describes the curvature of the fringes and it is linked with the number of odd numbered 5- and 7- membered carbon rings and the presence of lattice defects [8, 16, 35]. High tortuosity indicates a lower development of stacked layers [11, 36] and an increase in the sp^2/sp^3 hybridization [14] where sp^2 is related to the graphitic carbon and sp^3 to the organic carbon [19]. It is reported that tortuosity increases the separation between adjacent layers by limiting the development of the crystalline stack indicating the degree of disorder [13, 37]. In addition tortuosity is related to the availability of active sites [38]. Fringe tortuosity is obtained as the ratio of the fringe length divided by straight-line distance between the end points of the fringe [14].

An image processing methodology based on references [12, 16, 37] has been implemented in MATLAB® in order to process the particle micrographs, although in the literature other approaches have also been used [39]. The region of interest was selected manually, then the top-hat filtering was applied to correct uneven illumination [40] followed by a negative image transformation, histogram equalisation to improve the image contrast, binarisation (the threshold is calculated using Otsu's method), morphological operations (dilatation, opening, thickening and h-break) and skeletonisation. Disk elements of size 3 were used for the morphological operations. Also, a MATLAB® in-house code was developed for the calculation of the fringe length and the tortuosity. Fringes shorter than 0.47 nm (20 pixels according to the image scale used) were not considered for the analysis as they are thought to be unwanted features resisting the image cleaning process. This value is between the limits reported in the literature: 0.4 in [12, 41] and 0.5 in [16]. Figure 1 shows some examples of crystallites considered for analysis in the outer part of the primary particle (white ellipses in the Figure) formed by nearly flat graphene layers with certain periodicity. The outer ring of the primary particles where clear graphene stacks were observed was considered for analysis.

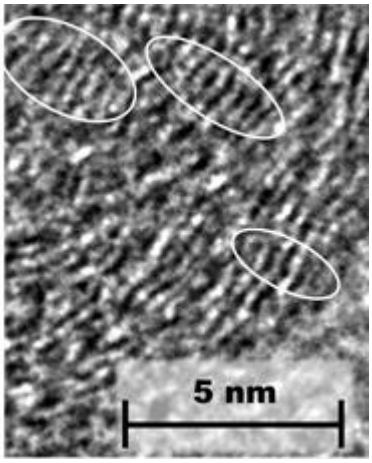

Figure 1. Example of graphene layers.

To assure the robustness of the obtained results, a one-sample non-parametric Kolmogorov Smirnov test in IBM statistical package for social sciences (SPSS) was performed. According to [16, 42] the interlayer spacing, crystallite length and tortuosity follow a log-normal distribution.

Although different techniques can be applied to characterise PM nanostructure, such as Raman or X-ray diffraction (XRD), TEM offers a direct measurement of the aforementioned parameters without intermediate processes [16] and is the only way to obtain soot tortuosity [12]. For instance, in [8], it is stated that the d_{002} obtained using TEM micrographs differs from the interlayer spacing obtained with Raman or XRD, however XRD provides an average value while TEM provides local values. L_a values obtained using TEM and XRD are compared in [11], although TEM measurements resulted in lower estimations, good agreement in the trends between both methods was found. In [12] it was concluded that HRTEM can be used as a standalone technique as the result obtained with Raman, XRD and HRTEM were in agreement. Despite the discrepancies in the values, all the techniques resulted in the same trends [8, 11].

2.2.3. Thermogravimetric analysis (TGA) methodology

A Perkin Elmer TGA model Pyris was employed to study soot oxidation characteristics. Whatman GF/F Glass microfiber 47 mm diameter filters were pre-heated at 600ºC during 6 hours to limit any influence of filter material losses during the desorption of volatile material during the nitrogen phase of the program. After this thermal pre-treatment, the filters were placed into a filter holder in the exhaust and loaded for one hour. In order to avoid any loss of PM during the sampling process, instead of scratching the filters, a sharp cylindrical hollow pipe was used to cut the filters at the same diameter as the TGA pan. The TGA program is divided in two phases depending on the atmosphere used: i) a nitrogen phase to remove the volatile organic fraction and ii)an air stage using a heating ramp of 3 °C/min. Further details of the methodology can be found in [28, 43].

3. RESULTS AND DISCUSSION

3.1. Nanostructure general characteristics

For all the conditions analysed, the micrographs show an onion-like or core-shell structure, characteristic of diesel engine particles. The inner core presents a disordered structure. In reference [16], it is suggested that this inner part of the primary particle is composed of several individual cores covered by carbon layers. The presence of several cores in a single particle suggests, according to the diesel literature, a rapid soot formation and coalescence of the particles during the formation process [26]. The outer shell is formed, to a large extent, by more or less parallel graphene lamellae, although some amorphous parts can be observed, with clear fringes although not formed by a large number of stacks and not well ordered, as previously reported in the GDI literature [19]. Furthermore, an amorphous outer ring of around 5 nm thickness has been reported for GDI particles collected from the engine oil [24]. In this investigation, the inner core diameter ranged between 6 and 16 nm and the outer graphene layer between 6 and 13 nm. However, the presence of this amorphous outer ring has not been observed. An example of the soot structure is shown in Figure 2.

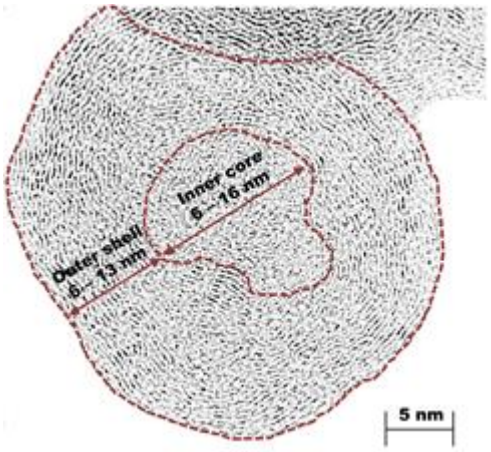

Figure 2. GDI particle nanostructure schematic.

Representative examples of particle micrographs obtained in TEM and corresponding to the analysis of particles from the engine operation with noEGR, EGR and REGR at both injection timings are given in Figure 3**Error! Reference source not found.**.

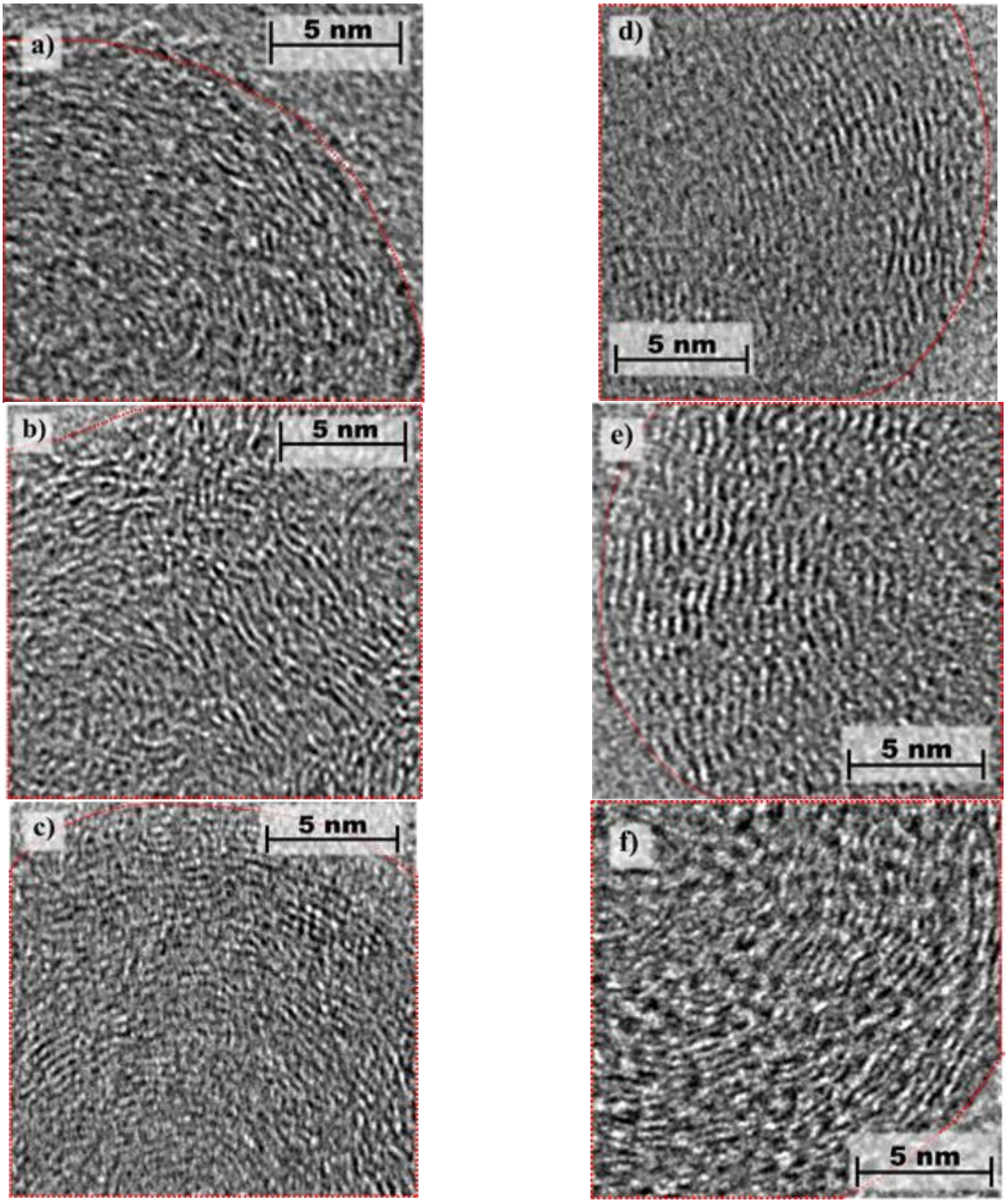

Figure 3. Example of TEM micrograph for ECU settings (303 CAD bTDC) a) baseline b)EGR c) REGR, and advanced injection timing (335 cAD bTDC) d) baseline e) EGR f) REGR. The borders of the particles have been marked for clarity

3.2.EGR/REGR influence on soot nanostructure parameters

The interlayer spacing results are presented in Figure 4, the average value together with the standard deviation is shown. The fringe length distributions are reported in Figure 5, tortuosity distribution in Figure 6 and a summary of all the values obtained for both fuel injection timings under noEGR, EGR and REGR conditions is presented in Table 3.

A slight tendency to increase d_{002} was observed for advanced injection timing (0.4110 nm) compared to ECU settings (0.3981 nm), Figure 4. However, the change in the fuel injection timing did not have any impact on the soot fringe length and tortuosity. The interlayer spacing results are in agreement with the trends found in the work carried out by Miyashita et al. [25]. They concluded that the influence of the fuel injection timing on the interlayer spacing was not significant as the soot formation process remained the same and GDI soot is produced at relatively low temperatures without experiencing oxidation. This is consistent with [44], is the authors hypothesised that soot is formed near the walls at the end of the combustion where the temperature is 1350K, the lower limit for soot formation. Therefore, during the exhaust stroke the temperature is too low for soot oxidation [44] and not high enough to affect the soot nanostructure. Also in [44], it was found that the critical fuel/air equivalence ratio for soot formation in gasoline is between 1.3-1.4. In [19], it was reported that soot nanostructure reflects changes between rich in fuel and stoichiometric/lean conditions. No differences on soot nanostructure between lean and stoichiometric conditions were observed, suggesting that fuel-air mixture in stoichiometric conditions was close to homogeneous and increasing the air content did not affect the formation of fuel-rich areas. High load, rich conditions and late injection produced higher rich in fuel areas into which the soot formation critical equivalence ratio was exceeded leading to particles with higher tortuosity. Moreover the formation of C5 species in this rich region could increase the curvature of the layers.

The different engine configuration used between researchers (i.e. injector position, wall-guided, spray guided) and the fuel properties, can have an impact on PM formation and oxidation processes. In the GDI literature, the majority of the authors reporting nanostructure use side-mounted injectors [19, 24, 27]. Drake et al. [45] stated that comparison between engine configurations could be misleading, as the soot formation process in the combustion chamber will primarily depend upon the injection system and mixture formation strategy. In this current work, it is thought that advanced and baseline injection timings generate rich-areas by wall-impingement into which the soot formation process is not significantly different generating soot with similar nanostructure. Therefore, it seems that the rich

regions formed at advanced and stoichiometric conditions might be similar leading to these minor differences in soot nanostructure.

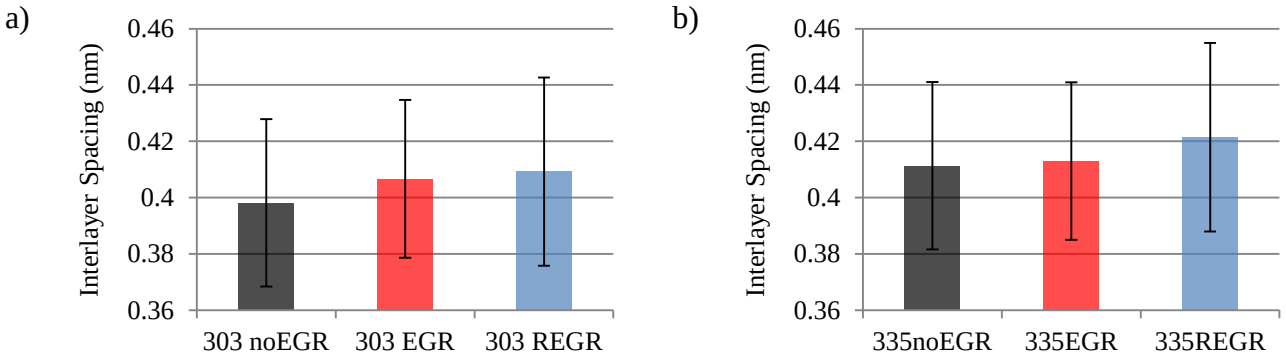

Figure 4. Interlayer spacing results for a) 303 CAD bTDC (ECU settings) and 335 CAD bTDC (advanced injection timing).

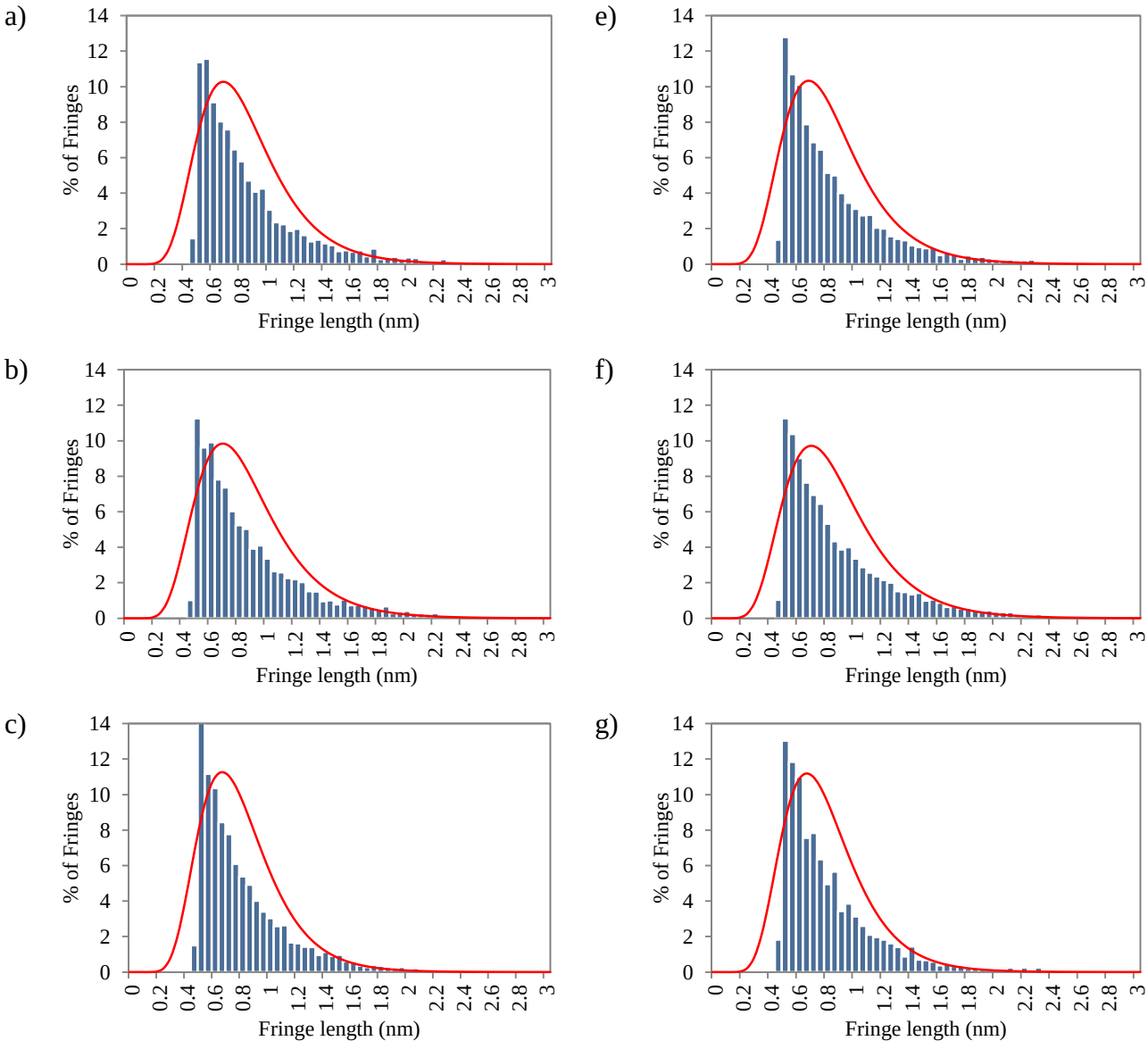

Figure 5. Fringe distribution for 303 CAD bTDC: a) baseline b) EGR c) REGR and 335 CAD bTDC: d) baseline e) EGR f) REGR

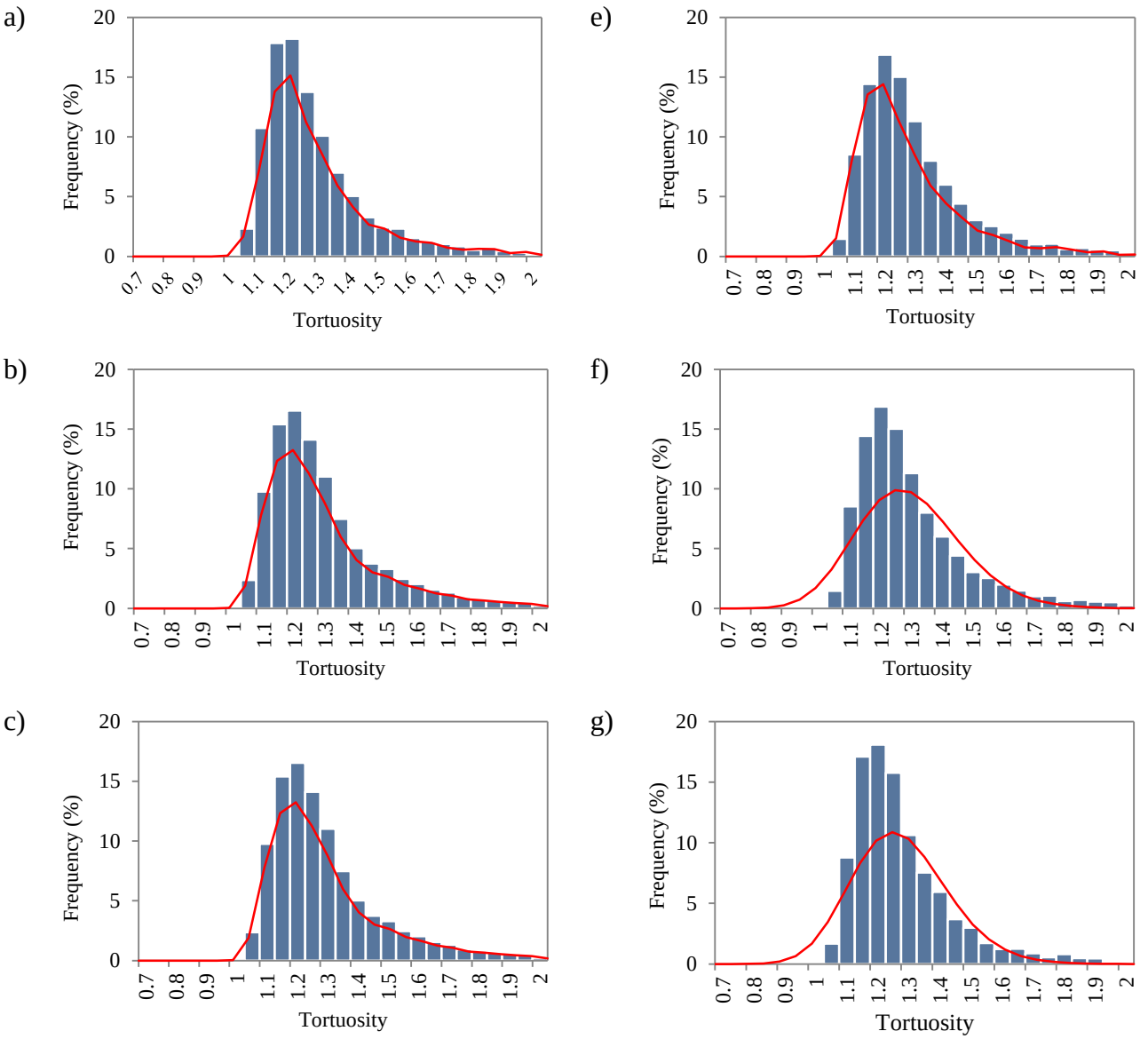

Figure 6. Tortuosity distribution for 303 CAD bTDC: a) baseline b) EGR c) REGR and 335 CAD bTDC: d) baseline e) EGR f) REGR

Table 4. Summary of nanostructural parameters a) 303 CAD bTDC and b) 335 CAD bTDC

a)	Baseline	EGR	REGR
d_{002}	0.398	0.408	0.409
L_a	0.845	0.869	0.804
τ	1.281	1.275	1.292

b)	Baseline	EGR	REGR
d_{002}	0.411	0.413	0.421
L_a	0.840	0.874	0.807
τ	1.279	1.298	1.278

EGR slightly increases d_{002} and the fringe length, although no significant trends in tortuosity have been found. Thus, the effect of EGR can be considered negligible. In [27] has been found that low percentages of EGR, 2.5%, can notably reduce the presence of the gas phase PAH, however, increasing EGR did not offer any further PAH reduction. On the other hand, no significant changes in

particulate-phase PAHs were observed. Five or more fused rings were predominantly adsorbed on soot cores [27]. Similar results are reported in the diesel literature, the lower combustion temperature from the use of EGR reduces the concentration of H radical and lowers the formation of PAHs and soot surface growth via the hydrogen abstraction acetylene addition mechanism [9]. In diesel engines, EGR has been reported to reduce the ordered arrangement of graphene lamellae, increasing d_{002} and reducing L_a [8]. The increase in d_{002}, was speculated to weaken the binding energy of the planes, leading to the increased likelihood of oxygen attack [8]. On the other hand, shorter fringes are associated to higher edge site carbon atoms than in the basal plane position and increasing reactivity [8]In [41], the use of EGR led to increased L_a and reduced tortuosity, parameters that were linked reduced soot reactivity. This behaviour was attributed to the production of soot with higher elemental carbon content under EGR conditions, a result of the longer combustion duration and reduced oxygen availability. These contradictory findings, suggest that the combination of dilution, thermal and chemical effects of EGR can affect soot nanostructure and oxidation differently depending on the engine condition and the setup arrangement. In GDI, this knowledge is still scarce.

For the GDI engine operation with REGR, the graphene lamellae interlayer spacing increases with respect to baseline and EGR engine operation and the crystalline length is reduced while tortuosity is not showing a clear trend. Hydrogen addition has been reported to reduce the size of the primary particles in an ethylene opposed jet counter diffusion flame [46]. It was concluded that hydrogen addition led to i) the formation of fullerenic nanostructure (curved carbon lamella), ii) increased rate of acetylene (a well-known precursor) oxidation through OH radical, which slows down benzene formation and therefore the development of large particles, iii) reduce soot surface growth through deactivation of soot surface site and iv) increase the formation rate of 5-membered ring PAH which curves the fringes. The effect of hydrogen on inhibiting/promoting the formation of gaseous unsaturated soot precursor species and single ring aromatics depends on the particular operating conditions and the relative proportions of the active species O, OH and H in the flame [47, 48]. For instance, the experimental and modelled results found for the specific case of methane laminar premixed flames [47] conclude that hydrogen could enhance the overall formation of unsaturated species and single-ring aromatic precursors of PAHs and soot. However, further research should be done to extrapolate those results to the case of turbocharged GDI engines where the reactants and turbulence levels are very different. In terms of PM concentration, hydrogen has been reported to significantly reduce the level of PM emitted [28, 49-51], its high diffusion coefficient enhances the air-fuel mixture, while the liquid fuel replacement as well as its high flame speed improve the

combustion process [48, 52]. Furthermore, the smaller quenching distance reduces the organic PM on account of the lower HCs available [50, 51].

According to the results obtained in this research work, Figure 4, Figure 5 and Figure 6, it seems that the injection timing (advanced or normal), EGR and REGR operation does not influence significantly soot nanostructure, although EGR and REGR globally modify the final emission of PM by promoting or reducing the formation of rich-in-fuel regions. It can be assumed that once the rich area is generated, the soot nanostructure will be similar and only by changing dramatically the formation process (i.e. stratified combustion mode) will have an impact in the final nanostructure. Generally, particle reactivity is influenced by several parameters including particle nanostructure, primary particle size, surface chemistry and chemical composition (i.e. carbonaceous, volatile material and ash). However, no changes in soot oxidation characteristics with EGR or REGR were observed in previous work [28], although small variations in the primary particle diameter were observed: baseline conditions (27 nm), EGR (23 nm) and REGR (25 nm) [53]. After thermogravimetric analysis (TGA), it was reported that the soot activation energy and the maximum mass loss rate were the same for baseline, EGR and REGR engine conditions, trends that are supporting the lack of changes in the soot nanostructure [28]. This is in agreement with the literature, as it has already been reported that GDI soot nanostructure is unaffected by the engine load and speed conditions, a finding that is reverse to diesel soot. This is attributed to the different combustion characteristics, as gasoline engines provide more consistent in-cylinder fuel-air mixture and flame temperatures.

3.3.Effect of TWC

It can be hypothesised that the relatively high temperatures in the TWC (between 650 -700°C) during typical engine operation with the presence of a catalyst could affect some of the PM physical properties. The interlayer spacing (Figure 7), fringe length (Figure 8) and tortuosity, (Figure 9) have been analysed pre and post the catalytic converter at both fuel injection timings. Table 5 reports the mean values of each parameter. The majority of the graphene lamellae is smaller than 1.2 nm peaking at 0.84 and present low tortuosity. These results are in agreement with previous GDI literature [26]. A negligible reduction after the TWC in the interlayer spacing and fringe length of the primary particles has been observed for both injection timings. At 335 CAD bTDC injection timing, the tortuosity falls from 1.278 to 1.25, while at 303 CAD bTDC there are no changes. However, in previous work [28], a 40% reduction in particle size distribution concentration at the TWC under advanced injection timing was measured, while at 303 CAD bTDC, almost no effect in the distribution was observed. The nature and quantity of the PM can be the reason for these findings. For advanced injection, PM concentration is ten times larger and composed mainly of soot, as

reported in the TGA analysis in [29]. Therefore, it is suggested that the soot is not oxidised but deposited in the three way catalyst by diffusion. Brownian diffusion has been reported to be the main mechanism involved for the deposition of small particles (<300 nm) [54, 55] as it is also pointed out in the GDI literature[23]. At 303 CAD bTDC, a high fraction of PM is composed of organic fraction, being heavy PAHs adsorbed onto the PM, which cannot be oxidised in the TWC. This is in agreement to the findings reported in [56], where it is claimed that the elemental carbon is unchanged in the TWC as well as the heavy PAHs adsorbed onto the PM.

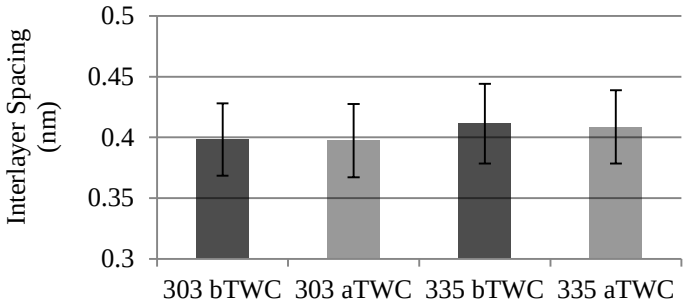

Figure 7. Effect of TWC on interlayer spacing

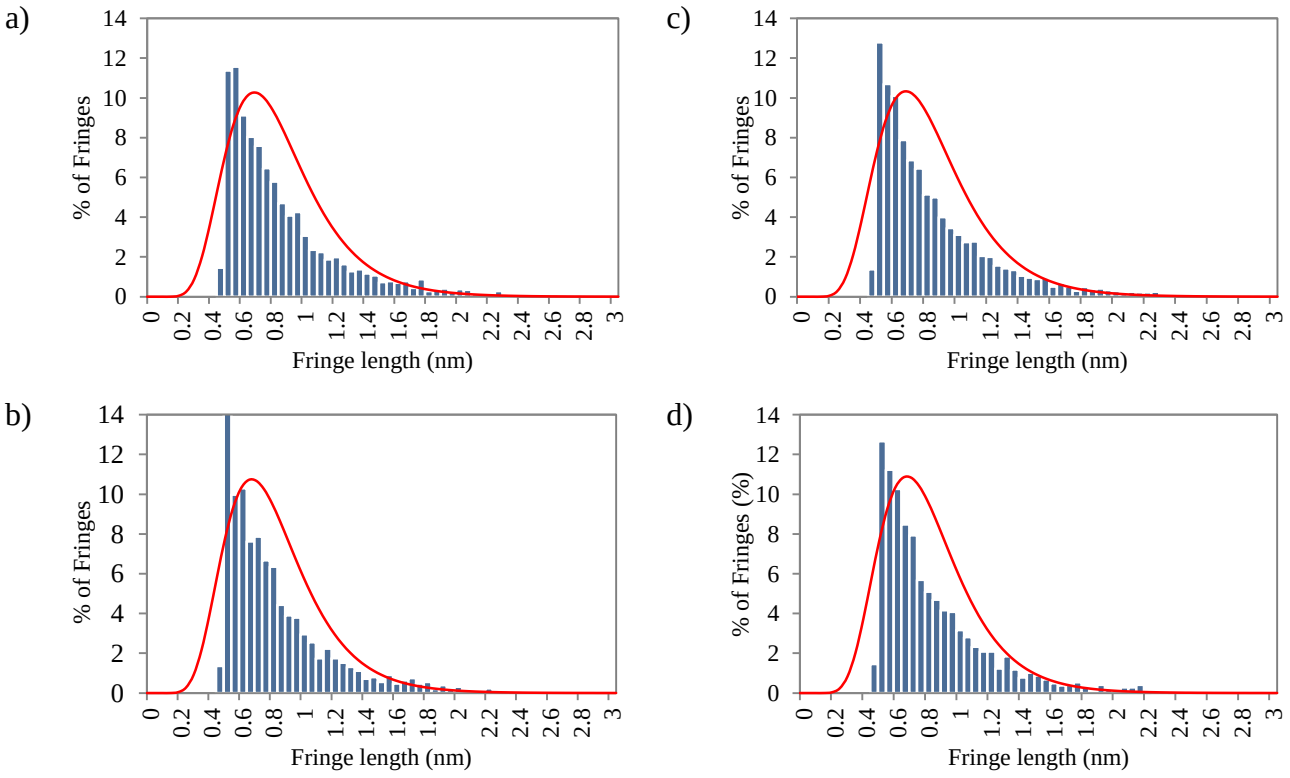

Figure 8. Length distribution for 303 CAD bTDC: a) bTWC b) aTWC and 335 CAD bTDC: c) bTWC d) aTWC

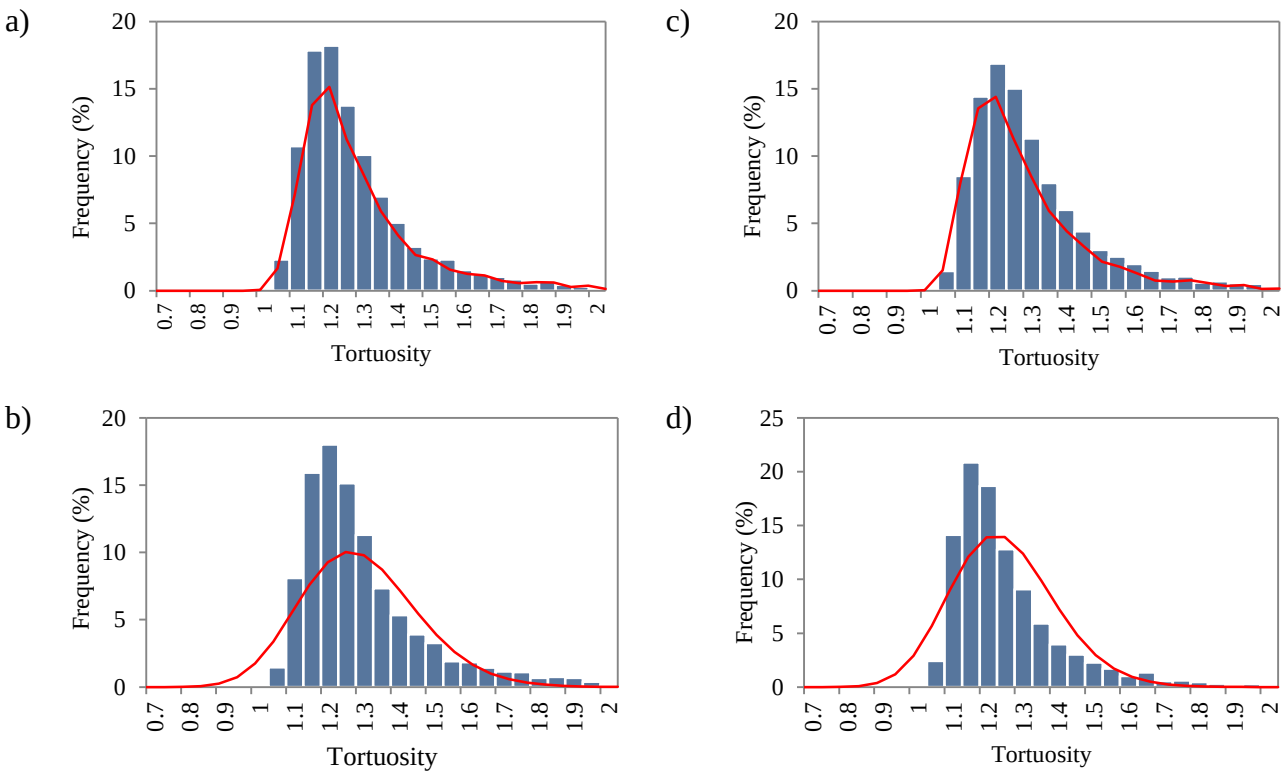

Figure 9. Tortuosity distribution for 303 CAD bTDC: a) bTWC b) aTWC and 335 CAD bTDC: c) bTWC d) aTWC

Table 5. Effect of TWC on nanostructure. Mean values.a)303 CAD bTDC and b) 335 CAD bTDC

a)	bTWC	aTWC
d_{002}	0.398	0.397
L_a	0.845	0.822
τ	1.281	1.293

b)	bTWC	aTWC
d_{002}	0.411	0.409
L_a	0.840	0.820
τ	1.279	1.250

The effect of the TWC on soot oxidation is presented in Figure 10. Although the maximum mass loss rate temperature after the TWC seems slightly shifted to lower temperatures, this is a mass artefact rather than an oxidative effect of the TWC. Until 480 °C, both curves have the same shape meaning that the activation energy and therefore, the reactivity are similar for both samples. Similar conclusions were found in a previous work for EGR and REGR soot oxidation behaviour [28]. It is hypothesised that the short residence time in the TWC is not enough to affect PM, although a reduced percentage can be deposited in the catalyst walls leading to the reduction observed by the SMPS aTWC in [28], therefore not affecting the soot nanostructure. However in [23], a strong influence of TWC on soot oxidation characteristics is found. This is attributed to the increased ash content after the catalytic converter and the higher organic content of the samples rather to any change in the nanostructural soot characteristics. It has been reported that the catalytic effect of ash depends on its

origin (e.g. lube oil metallic additives, engine wear and catalytic converters detachments) and formation conditions (combustion-derived ash precursors, unburned ash precursors and oxidation-derived ash in the filters). The high fraction of combustion-derived ash precursors downstream the TWC accelerates soot oxidation due to its metallic oxide nature and nano-level contact with soot particles [23].

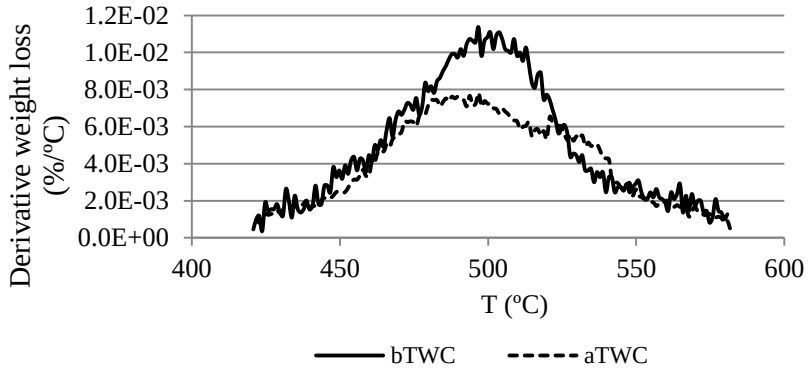

Figure 10. Effect of TWC on soot oxidative behaviour.

4. CONCLUSIONS

Soot from modern GDI engines have been characterised in this study. The effects of fuel injection timing and technologies such as EGR, REGR (i.e. hydrogen) and TWC on soot nanostructure features (interlayer spacing, fringe length and tortuosity) and soot oxidation have been analysed. Primary particles presented similar structure to diesel soot: i) an outer ring of ordered graphene layers between 6-13 nm thick and ii) an amorphous core of 6-16 nm diameter. While the PM nature (i.e. soot or organic) and concentration levels are influenced significantly by the changes of the fuel injection timing, EGR and REGR (including quantity and quality) the primary particle nanostructure is not affected. The interlayer spacing was between 0.398 and 0.411 nm, while the majority of the graphene lamellae fringe length was below 1.2 nm with an average of 0.82 nm. Little curvature has been observed for all the conditions analysed. The lack of effect in soot nanostructure attributed to homogeneous gasoline combustion process where the soot formation process is produced late in the combustion event at relatively low temperatures where no soot oxidation is promoted. This trend is opposite to the case of diesel combustion, in which injection settings and EGR produced a noticeable effect on soot nanostructure. In addition, the TWC did not lead to changes in the soot nanostructural features. rom the analysis presented here no differences in soot oxidation parameters have been observed in this research under EGR, REGR or TWC. This new finding adds to the knowledge that under stoichiometric gasoline combustion the primary particles nanostructure cannot be influenced..

Further research is needed to identify potential parameters that could modify the soot nanostructure and facilitate the soot oxidation process for the optimisation of the regeneration of the Gasoline Particulate Filter.

ACKNOWLEDGMENTS

The authors would like to thank EPSRC (Grant No: 1377213) for providing a scholarship to Maria Bogarra and Johnson Matthey for supporting the project. Innovate UK (Technology Strategy Board) is acknowledged for supporting this work with the project "CO_2 Reduction through Emissions Optimisation" (CREO: ref. 400176/149). The Advantage West Midlands and the European Regional Development Fund as part of the Science City Research Alliance Energy Efficiency Project are also acknowledged for supporting the research work. F.J. Martos expresses thanks to the government of Spain for supporting his research stay with the reference PRX15/00256 at the University of Birmingham.

DEFINITIONS, ACRONYMS, ABBREVIATIONS

d_{002}	Interlayer Spacing
L_a	Crystallite width
L_c	Crystallite height
κ	Number of layers per stack
τ	Tortuosity
aTWC	After Three Way Catalyst
bTDC	Before Top Dead Centre
bTWC	Before Three Way Catalyst
CAD	Crank angle degree
ECU	Electronic Computer Unit
EGR	Exhaust Gas Recirculation
GDI	Gasoline Direct Injection
GPFs	Gasoline Particulate Filters
HRTEM	High Resolution Transmission Electron Microscope
IMEP	Indicated Mean Effective Pressure
NEDC	New European Driving Cycle
PAHs	Polyaromatic Hydrocarbons
PM	Particulate Matter
REGR	Reformed Exhaust Gas Recirculation
SMPS	Scanning mobility particle sizer
TEM	Transmission Electron Microscope
TGA	Thermogravimetric analysis
TWC	Three Way Catalyst
XRD	X-Ray Diffraction

REFERENCES

1. *Regulation (EU) No 333/2014 of the European Parliament and of the Council of 11 March 2014 amending Regulation (EC) No 443/2009 to define the modalities for reaching the 2020 target to reduce CO2 emissions from new passenger cars*.

2. Zhao, F., M.C. Lai, and D.L. Harrington, *Automotive spark-ignited direct-injection gasoline engines.* Progess in Energy and Combustion Science, 1999. **25**: p. 437-562.
3. *Internation Agency for Research on Cancer: Outdoor air pollution a leading environmental cause of cancer deaths.* Press Release Nº221, 2013.
4. Donaldson, K., et al., *Role of inflammation in cardiopulmonary health effects of PM.* Toxicol Appl Pharmacol, 2005. **207**(2): p. 483-488.
5. Kim, K.H., E. Kabir, and S. Kabir, *A review on the human health impact of airborne particulate matter.* Environ. Int., 2015. **74**: p. 136-143.
6. Mamakos, A., et al., *Feasibility of Introducing Particulate Filters on Gasoline Direct Injection Vehicles, JRC Scientific and Policy Report, JRC68675, EUR 25297 EN, EU Commission.* 2011.
7. Saito, C., et al., *New Particulate Filter Concept to Reduce Particle Number Emissions.* SAE Technical Paper, 2011. **2011-01-0814**.
8. Al-Qurashi, K. and A.L. Boehman, *Impact of exhaust gas recirculation (EGR) on the oxidative reactivity of diesel engine soot.* Combustion and Flame, 2008. **155**(4): p. 675-695.
9. Al-Qurashi, K., A.D. Lueking, and A.L. Boehman, *The deconvolution of the thermal, dilution, and chemical effects of exhaust gas recirculation (EGR) on the reactivity of engine and flame soot.* Combustion and Flame, 2011. **158**(9): p. 1696-1704.
10. Yehliu, K., et al., *Impact of engine operating modes and combustion phasing on the reactivity of diesel soot.* Combustion and Flame, 2013. **160**(3): p. 682-691.
11. Yehliu, K., et al., *Impact of fuel formulation on the nanostructure and reactivity of diesel soot.* Combustion and Flame, 2012. **159**(12): p. 3597-3606.
12. Yehliu, K., R.L. Vander Wal, and A.L. Boehman, *A comparison of soot nanostructure obtained using two high resolution transmission electron microscopy image analysis algorithms.* Carbon, 2011. **49**(13): p. 4256-4268.
13. Vander Wal, R.L., et al., *Analysis of HRTEM images for carbon nanostructure quantification.* Journal of Nanoparticle Research, 2005. **6**(6): p. 555-568.
14. Li, Z., et al., *Evolution of the nanostructure, fractal dimension and size of in-cylinder soot during diesel combustion process.* Combustion and Flame, 2011. **158**(8): p. 1624-1630.
15. Song, J., et al., *Examination of the oxidation behavior of biodiesel soot.* Combustion and Flame, 2006. **146**(4): p. 589-604.
16. Gaddam, C.K., C.-H. Huang, and R.L. Vander Wal, *Quantification of nano-scale carbon structure by HRTEM and lattice fringe analysis.* Pattern Recognition Letters, 2016. **76**: p. 90-97.
17. Vander Wal, R.L., V.M. Bryg, and M.D. Hays, *Fingerprinting soot (towards source identification): Physical structure and chemical composition.* Journal of Aerosol Science, 2010. **41**(1): p. 108-117.
18. Mühlbauer, W., et al., *Correlations between physicochemical properties of emitted diesel particulate matter and its reactivity.* Combustion and Flame, 2016. **167**: p. 39-51.
19. Gaddam, C.K. and R.L. Vander Wal, *Physical and chemical characterization of SIDI engine particulates.* Comb. Flame, 2013. **160**(11): p. 2517-2528.
20. Uy, D., et al., *Characterization of gasoline soot and comparison to diesel soot: Morphology, chemistry, and wear.* Tribology International, 2014. **80**: p. 198-209.
21. Wang-Hansen, C., et al., *Characterization of Particulate Matter from Direct Injected Gasoline Engines.* Topics in Catalysis, 2013. **56**(1-8): p. 446-451.
22. Seong, H., K. Lee, and S. Choi, *Effects of Engine Operating Parameters on Morphology of Particulates from a Gasoline Direct Injection (GDI) Engine.* SAE Technical Paper, 2013. **2013-01-2574**.
23. Choi, S. and H. Seong, *Oxidation characteristics of gasoline direct-injection (GDI) engine soot: Catalytic effects of ash and modified kinetic correlation.* Comb. Flame, 2015. **162**(6): p. 2371-2389.
24. La Rocca, A., et al., *Characterisation of soot in oil from a gasoline direct injection engine using Transmission Electron Microscopy.* Tribology International, 2015. **86**: p. 77-84.
25. Miyashita, K., et al., *TEM Analysis of Soot Particles Sampled from Gasoline Direction Injection Engine Exhaust at Different Fuel Injection Timings.* SAE Technical Paper 2015. **2015-01-1872**.
26. Liati, A., et al., *Electron microscopic characterization of soot particulate matter emitted by modern direct injection gasoline engines.* Combustion and Flame, 2016. **166**: p. 307-315.
27. An, Y.Z., et al., *An experimental study of polycyclic aromatic hydrocarbons and soot emissions from a GDI engine fueled with commercial gasoline.* Fuel, 2016. **164**: p. 160-171.

28. Bogarra, M., et al., *Reformate Exhaust Gas Recirculation Effect on Particulate Matter, Soot Oxidation and Three Way Catalyst Performance in Gasoline Direct Injection Engines.* SAE Int. J. Engines, 2015. **9**(1).
29. Gomes, S.R., et al., *Thermodynamic and experimental studies of catalytic reforming of exhaust gas recirculation in gasoline engines.* Applied Catalysis B: Environmental, 2011. **102**(1-2): p. 44-53.
30. Fennell, D., et al., *Thermochemical recovery technology for improved modern engine fuel economy – part 1: analysis of a prototype exhaust gas fuel reformer.* RSC Adv., 2015. **5**(44): p. 35252-35261.
31. Bogarra, M., et al., *Study of particulate matter and gaseous emissions in gasoline direct injection engine using on-board exhaust gas fuel reforming.* Applied Energy, 2016. **180**: p. 245-255.
32. Liati, A., et al., *Variations in diesel soot reactivity along the exhaust after-treatment system, based on the morphology and nanostructure of primary soot particles.* Combustion and Flame, 2013. **160**(3): p. 671-681.
33. Iwashita, N. and M. Inagaki, *Relations between structural parameters obtained by X-Ray powder diffraction of various carbon materials.* Carbon, 1993. **31**(7): p. 1107-1113.
34. Takagi, H., et al., *XRD analysis of carbon stacking structure in coal during heat treatment.* Fuel, 2004. **83**(17-18): p. 2427-2433.
35. Vander Wal, R.L. and A.J. Tomasek, *Soot nanostructure: dependence upon synthesis conditions.* Combustion and Flame, 2004. **136**(1-2): p. 129-140.
36. Radovic, L.R., P.L. Walker, and R.G. Jenkins, *Importance of carbon active sites in the gasification of coal chars.* Fuel, 1983. **62**(7): p. 849–856.
37. Yehliu, K., R.L. Vander Wal, and A.L. Boehman, *Development of an HRTEM image analysis method to quantify carbon nanostructure.* Combustion and Flame, 2011. **158**(9): p. 1837-1851.
38. Raj, A., et al., *Structural effects on the oxidation of soot particles by O2: Experimental and theoretical study.* Combustion and Flame, 2013. **160**(9): p. 1812-1826.
39. Toth, P., et al., *Quantitative differentiation of poorly ordered soot nanostructures: A semi-empirical approach.* Fuel, 2012. **99**: p. 1-8.
40. Gonzalez, R.C. and R.E. Woods, *Digital Image Processing (3rd Edition)*. 2006: Prentice-Hall, Inc.
41. Li, X., et al., *Impact of exhaust gas recirculation (EGR) on soot reactivity from a diesel engine operating at high load.* Applied Thermal Engineering, 2014. **68**(1-2): p. 100-106.
42. Tian, K., et al., *Determination of the morphology of soot aggregates using the relative optical density method for the analysis of TEM images.* Combustion and Flame, 2006. **144**(4): p. 782-791.
43. Wang, C., et al., *Fuel Effect on Particulate Matter Composition and Soot Oxidation in a Direct-Injection Spark Ignition (DISI) Engine.* Energy & Fuels, 2014. **28**(3): p. 2003-2012.
44. Hageman, M.D., S.S. Sakai, and D.A. Rothamer, *Determination of soot onset and background particulate levels in a spark-ignition engine.* Proceedings of the Combustion Institute, 2015. **35**(3): p. 2949-2956.
45. Drake, M., et al., *Piston Fuel Films as a Source of Smoke and Hydrocarbon Emissions from a Wall-Controlled Spark-Ignited Direct-Injection Engine,*. SAE Technical Paper 2003. **2003-01-0547**.
46. Choi, J.H., et al., *Impacts of hydrogen addition on micro and nanostructure of soot particles formed in C2H4/air counter diffusion flames.* International Journal of Hydrogen Energy, 2016(35): p. 15852-15858.
47. Mze Ahmed, A., et al., *Experimental and numerical study on rich methane/hydrogen/air laminar premixed flames at atmospheric pressure: Effect of hydrogen addition to fuel on soot gaseous precursors.* International Journal of Hydrogen Energy, 2016. **41**(16): p. 6929-6942.
48. Verhelst, S. and T. Wallner, *Hydrogen-fueled internal combustion engines.* Progress in Energy and Combustion Science, 2009. **35**(6): p. 490-527.
49. Fennell, D., et al., *GDI Engine Performance and Emissions with Reformed Exhaust Gas Recirculation (REGR).* SAE Technical Paper, 2013. **2013-01-0537**.
50. Zhao, H., R. Stone, and L. Zhou, *Analysis of the particulate emissions and combustion performance of a direct injection spark ignition engine using hydrogen and gasoline mixtures.* International Journal of Hydrogen Energy, 2010. **35**(10): p. 4676-4686.
51. Stone, R., H. Zhao, and L. Zhou, *Analysis of Combustion and Particulate Emissions when Hydrogen is Aspirated into a Gasoline Direct Injection Engine.* SAE Technical Paper, 2010. **2010-01-0580**.

52. Fennell, D., J. Herreros, and A. Tsolakis, *Improving gasoline direct injection (GDI) engine efficiency and emissions with hydrogen from exhaust gas fuel reforming.* International Journal of Hydrogen Energy, 2014. **39**(10): p. 5153-5162.
53. Bogarra, M., et al., *Impact of Exhaust Gas Fuel Reforming and Exhaust Gas Recirculation on Particulate Matter Morphology in Gasoline Direct Injection Engine.* Journal of Aerosol Science, 2016.
54. Yang, J., et al., *Single wall diesel particulate filter (DPF) filtration efficiency studies using laboratory generated particles.* Chemical Engineering Science, 2009. **64**(8): p. 1625-1634.
55. Hayashi, H. and S. Kubo, *Computer simulation study on filtration of soot particles in diesel particulate filter.* Computers & Mathematics with Applications, 2008. **55**(7): p. 1450-1460.
56. Johnson, T., *Vehicular Emissions in Review.* SAE International Journal of Engines, 2016. **9**(2).